

PAPER • OPEN ACCESS


# A study on influence of superparamagnetic iron oxide nanoparticles (SPIONs) on green gram (*Vigna radiata* L.) and earthworm (*Eudrilus eugeniae* L.)

To cite this article: Antony V Samrot *et al* 2020 *Mater. Res. Express* 7 055002

View the [article online](#) for updates and enhancements.

## Recent citations

- [Adsorption Efficiency of Chemically Synthesized Superparamagnetic Iron Oxide Nanoparticles \(SPIONs\) on Crystal Violet Dye](#)  
Antony V. Samrot *et al*
- [A review on synthesis, characterization and potential biological applications of superparamagnetic iron oxide nanoparticles](#)  
Antony V. Samrot *et al*



**ECS** The Electrochemical Society  
Advancing solid state & electrochemical science & technology  
2021 Virtual Education

**Fundamentals of Electrochemistry:**  
Basic Theory and Kinetic Methods  
Instructed by: **Dr. James Noël**  
Sun, Sept 19 & Mon, Sept 20 at 12h–15h ET

Register early and save!

# Materials Research Express



## PAPER

### OPEN ACCESS

RECEIVED  
27 December 2019

REVISED  
2 April 2020

ACCEPTED FOR PUBLICATION  
20 April 2020


PUBLISHED  
4 May 2020

Original content from this work may be used under the terms of the [Creative Commons Attribution 4.0 licence](#).

Any further distribution of this work must maintain attribution to the author(s) and the title of the work, journal citation and DOI.



## A study on influence of superparamagnetic iron oxide nanoparticles (SPIONs) on green gram (*Vigna radiata* L.) and earthworm (*Eudrilus eugeniae* L.)

Antony V Samrot<sup>1,5</sup> , SaiPriya C<sup>2</sup>, Jenifer Selvarani A<sup>2</sup>, Venket Subbu R<sup>2</sup>, Jane Cypriyana P J<sup>2</sup>, Lavanya Y<sup>2</sup>, Shehanaz Afreen R<sup>2</sup>, Soundarya P<sup>2</sup>, Sherly Priyanka R B<sup>2</sup>, Sangeetha P<sup>2</sup>, Reji Joseph Varghese<sup>2</sup> and Suresh Kumar S<sup>3,4,5</sup>

<sup>1</sup> School of Bioscience, Faculty of Medicine, Bioscience and Nursing, MAHSA University, 42610 Jenjarom, Selangor, Malaysia

<sup>2</sup> Department of Biotechnology, School of Bio and Chemical Engineering, Sathyabama Institute of Science and Technology, Chennai 600119, Tamil Nadu, India

<sup>3</sup> Department of Medical Microbiology and Parasitology, Universiti Putra Malaysia, 43400 UPM Serdang, Selangor, Malaysia

<sup>4</sup> Department of Cancer, Institute of Bioscience, Universiti Putra Malaysia, Malaysia

<sup>5</sup> Authors to whom any correspondence should be addressed.

E-mail: [antonyamrot@gmail.com](mailto:antonyamrot@gmail.com) and [sureshkudsc@gmail.com](mailto:sureshkudsc@gmail.com)

**Keywords:** SPIONs, bioaccumulation, toxicity, ICP-OES

### Abstract

Nanoparticles usage are now emerging as hazardous nanopollutants due to inappropriate usage and improper disposal. Superparamagnetic Iron Oxide Nanoparticles (SPIONs) is a widely used nanoparticle with various applications. In this study, SPIONs was evaluated for its impact against *Vigna radiata* and *Eudrilus eugeniae*. SPIONs were synthesized by chemical co-precipitation method in presence of cobalt chloride. The produced SPIONs was characterized using UV-Visible Spectroscopy, SEM (Scanning electron microscopy), EDX (Energy dispersive X-ray spectroscopy), XRD (X-ray diffraction), TEM (Transmission electron microscopy), AFM (Atomic force microscopy), XPS (X-ray photoelectron spectroscopy) and Zeta potential. The synthesized SPIONs were crystalline and monodispersed with size ranging between 15 nm and 20 nm. The seedlings of SPIONs treated *Vigna radiata* were found to have reduced root and shoot growth. The bioaccumulation of iron oxide in the treated plants was confirmed by ICP-OES (Inductively coupled plasma - optical emission spectrometry) analysis and Prussian blue staining. Cellular destruction and reduced reproduction rate were found in SPIONs exposed *Eudrilus eugeniae* and ICP-OES analysis of earthworm samples affirmed the bioaccumulation of SPIONs.

### 1. Introduction

Nanotechnology is a blooming field of science and has variety of applications in the field of science (Kreuter *et al* 2003). Applications of nanoparticles in various fields include agriculture, drug delivery (Samrot *et al* 2019a), imaging (Justin *et al* 2017, Justin *et al* 2018, Sruthi *et al* 2018, Samrot *et al* 2018a), mosquito larvicidal activity (Samrot *et al* 2019b), environmental remediation (Samrot *et al* 2019c), bioactivity including anticancer and antibacterial activity (Samrot *et al* 2016, Samrot *et al* 2018b, Samrot *et al* 2019a). The increased usage creates demand in the production alleviating the risks associated with improper disposal of metal nanoparticles. Several studies have assessed the negative impacts of inappropriate nanoparticle disposal in the environment (Taghavi *et al* 2013). Nanoparticles cause cell damage when they get accumulated inside cells by inducing oxidative stress, DNA damage and apoptosis (Ahamed *et al* 2010). The toxicity of the nanoparticles depends on the size, shape, surface chemistry, degree of internalization, dosage etc (Sharifi *et al* 2012). Nanoparticles when disposed in soil or water are unseeingly not readily metabolized by plants and so get accumulated in them. When these plants are consumed by animals/human, the particles enter the next trophic level leading to biomagnification. SPIONs in turn are biocompatibility and hence they can be used in targeted drug delivery as they can be directed to site such as an organ or tumor by applying

external magnetic field (Yang *et al* 2008). They are also used in a wide range of biomedical applications like MRI scanning (Bulte and Kraitchman 2004), magnetic isolation of cells etc (Xu *et al* 2011). SPIONs can bind to drug, protein, antibody, enzymes however the uptake of SPIONs by the cells depends on the type of cells (Osaka *et al* 2009).

Since the SPIONs are versatile and explored in various fields, there exists a pressing need to meticulously observe the impact it creates in the living system to alleviate the potential risks connected with indecent disposal. Consequently we present our report on the SPIONs prepared by chemical co-precipitation method in the presence of cobalt, and its characteristics well documented by instrumental analysis. And look for their impact against a plant model, *Vigna radiata* and an animal model, *Eudrilus eugeniae*. *E. eugeniae* was taken as test model for its faster productivity, low cost and easy maintenance (Butt and Lowe 2010).

## 2. Materials and methods

### 2.1. Materials

Ammonia solution, cobalt chloride hexahydrate, ferric chloride hexahydrate, ferrous sulphate heptahydrate and sodium hydroxide were purchased with extrapure from SRL, India. Sodium hypochlorite was purchased from M/s Merck, India. Nitrogen purged Millipore water was used for the nanoparticle synthesis.

### 2.2. Synthesis of SPIONs

100 ml of 1 M ferric chloride ( $\text{FeCl}_3 \cdot 6\text{H}_2\text{O}$ ) and 1 M of ferrous sulphate ( $\text{FeSO}_4 \cdot 7\text{H}_2\text{O}$ ) were mixed together. A solution of  $\text{CoCl}_2$ -NaOH was prepared with 50 ml 1 M cobalt chloride hexahydrate ( $\text{CoCl}_2 \cdot 6\text{H}_2\text{O}$ ) and 50 ml 5 M sodium hydroxide. To the precursor iron solution, 100 ml of  $\text{CoCl}_2$ -NaOH mixture was added in drops with vigorous stirring maintained at 60 °C. To these drops of ammonia was added until the contents turn black. Precipitates collected in external magnetic field were washed several times with Nitrogen purged Millipore water and lyophilized.

### 2.3. Characterization of SPIONs

SPIONs were characterized to understand their chemical and structural properties. The absorption profile of the nanoparticles was checked in UV visible spectrum using UV-vis (Shimadzu). The size and chemical composition of the nanoparticles were checked through SEM and EDX. Further the size precision was measured through TEM (TEECNAI G2 Spirit Biotwin—120 kV). The confinement of the nanoparticle to the three coordinates as 3D images were noted by AFM (Bruker, Germany). The particulate nature of the SPIONs were recorded in the  $2\theta$  range of 20°–80° in a fixed-time mode at room temperature using Smartlab X-ray diffractometer (Rigaku, Japan) and the stability of the SPIONs was examined by zeta potential (Brookhaven Zeta-PALS).

### 2.4. Exposure study of SPIONs on plant model, *Vigna radiata*

#### 2.4.1. Pretreatment of seeds

The seeds of *Vigna radiata* were surface sterilized with 2 % sodium hypochlorite solution and were soaked overnight in distilled water. The soaked seeds were again surface sterilized before use.

#### 2.4.2. Treatment of seeds with SPIONs

The impact analysis of the SPIONs on *Vigna radiata* was carried out for a study period of 6 days. The SPIONs sample were diluted with distilled water for the hydroponic culturing to a working concentrations of  $1 \mu\text{g ml}^{-1}$ ,  $10 \mu\text{g ml}^{-1}$  and  $20 \mu\text{g ml}^{-1}$ . The seeds were allowed to germinate and grown *in-vitro* using culture tubes containing SPIONs with no other nutrient. Each culture tube was introduced with pretreated seeds containing a M-shaped paper inserts (Whatmann filter paper) in order to keep them in contact with the SPIONs solution. The seed germination and growth were observed for the study concentrations in triplicates with distilled water as control.

#### 2.4.3. Growth and biomass measurement

The germinated seeds were checked for their root and shoot length on the 3<sup>rd</sup> and 6<sup>th</sup> day. The total weight of the plants on the 6th day was measured to evaluate their biomass.

#### 2.4.4. Qualitative phytochemical analysis

2 g of the plant was crushed with 15 ml of distilled water using mortar and pestle. The puree was filtered using Whatmann Filter paper. The filtrate was used to assess the presence of the following phytochemical test.

##### 2.4.4.1. Test for carbohydrates

Few drops of Molisch's reagent was added to the extract and along with concentrated  $\text{H}_2\text{SO}_4$ . Formation of red color confirmed the presence of carbohydrates (Kumari *et al* 2016).

#### 2.4.4.2. Test for proteins

The aqueous extract was added to 1 ml NaOH and 1% CuSO<sub>4</sub> and appearance of violet color stood positive for proteins (Kumari *et al* 2016).

#### 2.4.4.3. Test for lipids

2 ml of aqueous extract was added to 0.5 N KOH (prepared in ethanol) with few drops of phenolphthalein and heated in water bath for an hour. Soap formation confirmed the presence of lipids (Praveen and Nair 2014).

#### 2.4.4.4. Test for tannins

The aqueous extract when added to 0.5 ml of 10 % FeCl<sub>3</sub>, formation of brownish blue color confirmed the presence of tannins (Edeoga *et al* 2005, Samrot *et al* 2010).

#### 2.4.4.5. Test for saponins

The extract was mixed with distilled water and shaken vigorously forms honey comb froth confirmed the occurrence of saponins (Ezeonu and Ejikeme 2016).

#### 2.4.4.6. Test for alkaloids

The acidic plant extract treated with 0.5 ml Dragendroff's reagent forms red color precipitates indicative of alkaloids (Samrot *et al* 2019).

#### 2.4.4.7. Test for flavonoids

2 ml extract added to 0.5 ml NaOH formed a yellow colored solution, which disappeared with 70 % HCl indicated the presence of flavonoids. (Samrot *et al* 2019).

#### 2.4.4.8. Test for phenols

The test solution turning blue color when 5% FeCl<sub>3</sub> was added to the extract indicated the presence of phenols (Samrot *et al* 2019).

#### 2.4.4.9. Test for cardiac glycosides

1 ml extract mixed with 0.5 ml of glacial acetic acid with few drops of 1% FeCl<sub>3</sub> had brown ring at the interface indicated the presence of cardiac glycosides (Auwal *et al* 2014).

#### 2.4.5. Prussian blue staining of plant parts

The root tips, the basal region of shoot and the leaf apex of the plants after 6 days treatment were subjected to Prussian blue staining to identify iron elements present in the tissues. Equal volumes of freshly prepared 2% Potassium ferrocyanide and 2% Hydrochloric acid were mixed together to get Prussian blue staining buffer and the above mentioned plant parts were soaked in staining buffer separately for 15 min (Wei *et al* 2015). After incubation, they were rinsed in distilled water and thin sections of the sample was cut using a blade & scalpel and fixed on a glass slide to observe under Light microscope at 10 X magnification.

#### 2.4.6. ICP-OES analysis of *Vigna radiata*

SPIONs treated plants were rinsed in distilled water, dried and digested with 2 ml of nitric acid to obtain its acidic extract. The obtained extract was heated to 120 °C for 30 min and subjected for ICP–OES analysis to detect iron (Agilent ICP-OES VDV 51009) (Geisler-Lee *et al* 2012).

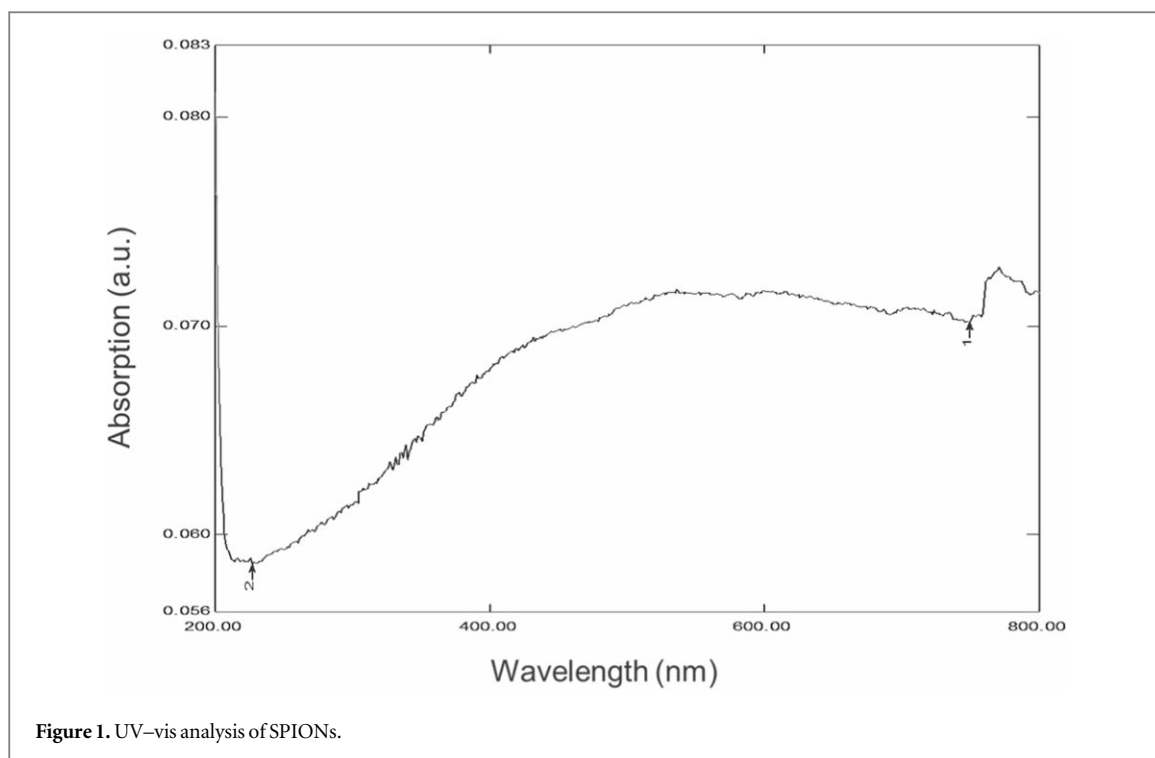
### 2.5. Exposure study of SPIONs on animal model, *Eudrilus eugeniae*

#### 2.5.1. Collection and pre-treatment of earthworms

The earthworm, *Eudrilus eugeniae* were collected from SS vermicompost, Tambaram, Chennai and were kept in manure rich soil. Prior to the nanoparticle exposure, they were allowed to adapt to the soil environment for 2 days. The moisture content was maintained and the Earthworms were fed with powdered cow dung every 24 h (Samrot *et al* 2017, Samrot *et al* 2019d). The earthworms were pretreated as mentioned earlier (Samrot *et al* 2017).

#### 2.5.2. Exposure of *Eudrilus eugeniae* with SPIONs

The pretreated earthworms were exposed to different concentrations of SPIONs (10 mg, 20 mg and 30 mg) added to soil, as per the same procedures followed in our earlier reports on gold nanoparticle by Samrot *et al* (2018c). A count of 20 earthworms was introduced to each of the study concentration. On the 10th day, the earthworms from each concentration was subjected to histology and ICP–OES analysis. Similar protocol was



trialed for all the SPIONs concentration to observe the impact on reproduction for a period of 30 days (Samrot *et al* 2017). Phenotypic changes in appearance and behavioral patterns were observed for each set of earthworms and compared to the control.

#### 2.5.3. Histology studies of *Eudrilus eugeniae*

On the 10th day, foregut, midgut and hindgut region of three earthworms from each concentration was cut using a surgical blade. Tissues were preserved in 10% formaldehyde solution, dehydrated in ethanol and then fixed in wax. Sections were made using microtome and H & E staining was performed. Sections were observed under microscope and histological images were documented.

#### 2.5.4. ICP-OES Analysis of *Eudrilus eugeniae*

After the study for 10 days, one earthworm from each concentration were dissected, digested in nitric acid (Samrot *et al* 2017, Samrot *et al* 2019b) and was subjected to elemental analysis for the presence of Fe using ICP-OES.

### 2.6. Statistical analysis

All the experiments were performed in triplicates and the mean value is represented as results.

## 3. Results

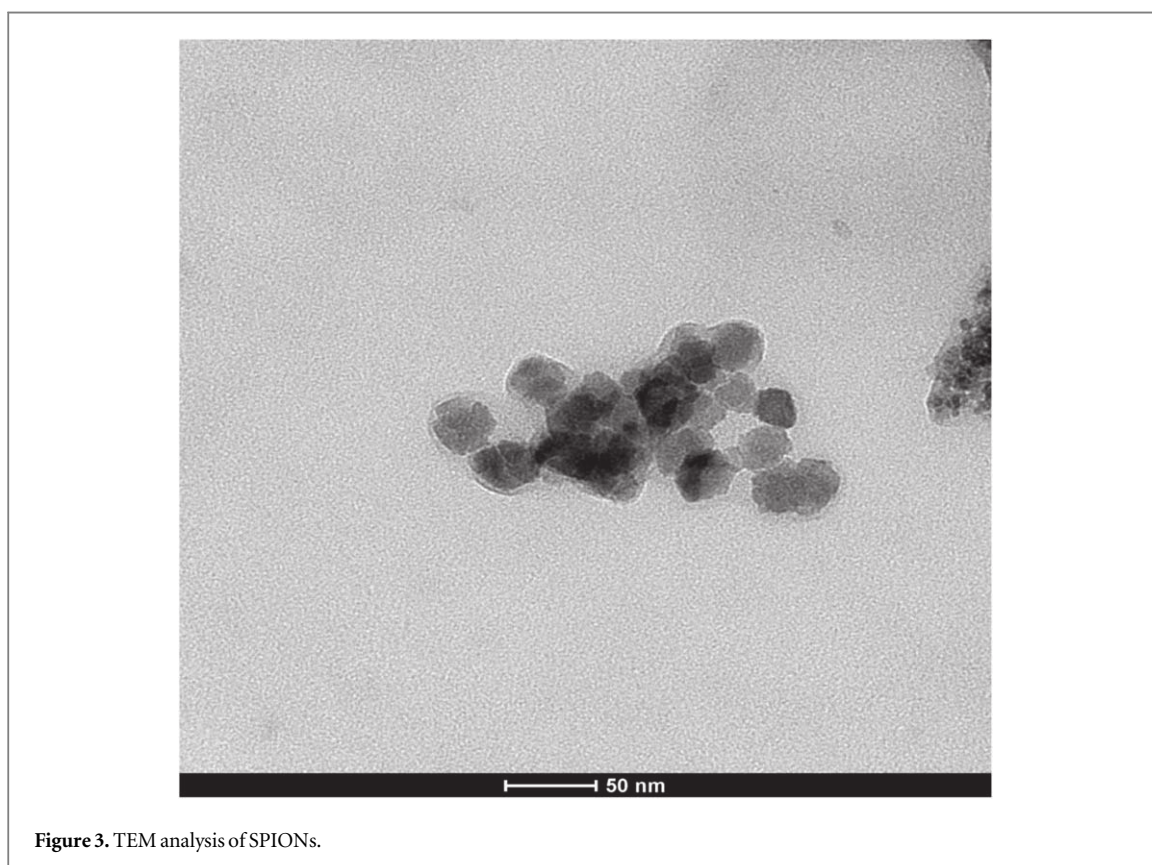
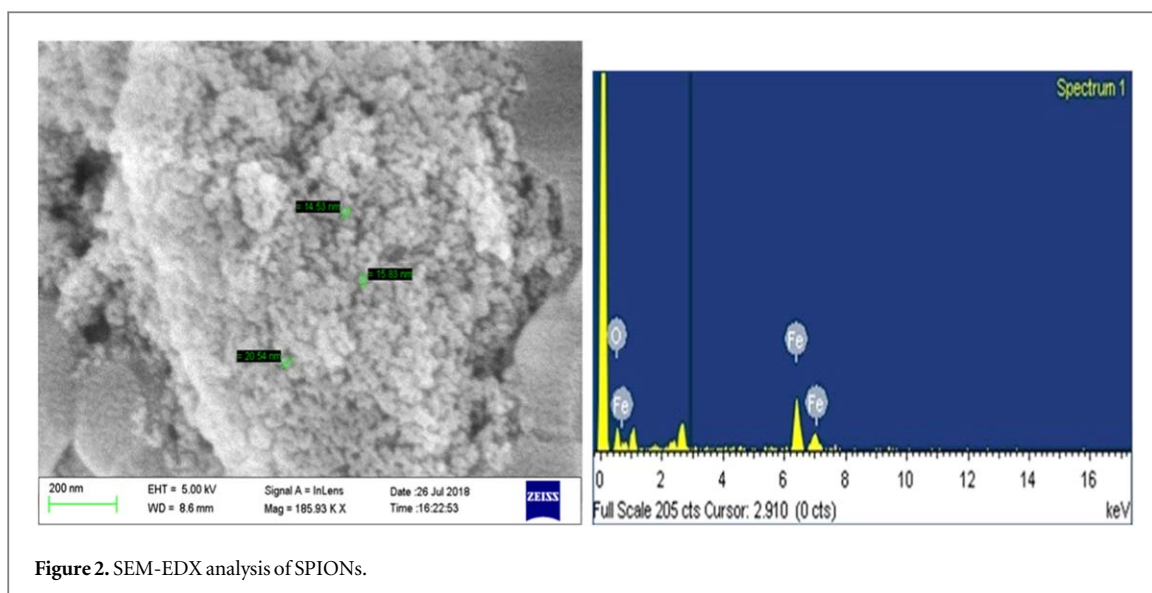
### 3.1. Characterization of SPIONs

#### 3.1.1. UV-vis

The absorbance property of the synthesized SPIONs can be understood on exposure to UV-Visible radiations. From the results, it is observed that the synthesized SPIONs show maximum absorbance near 420 nm followed by a blunt peak in the range of 450 nm–540 nm (figure 1). Kumar *et al* (2015) has stated that the absorption peak for  $\text{Fe}_3\text{O}_4$  appeared at 492 nm while Samrot *et al* (2017) reported peak absorbance near 250–260 nm for SPIONs, these discrepancies in the absorption spectra could be due to the varying size and composition of SPIONs as a contributing factor.

#### 3.1.2. SEM-EDX

Using SEM, the topographical view was visualized at the magnification of 185.93 KX where the synthesized SPIONs were in the size range of 14.53 nm to 20.54 nm (figure 2). Samrot *et al* (2019c) showed in his earlier discussions the size of SPIONs produced using ammonia as reducing agent was around 25 nm, whereas the use of a different reducing agent in this case Cobalt chloride in NaOH did contribute to the change in size of the



nanoparticle formation. EDX results affirmed the elemental composition of the synthesized SPIONs which showed the presence of Fe and O.

### 3.1.3. TEM

TEM images revealed the aggregation of synthesized SPIONs with particles appearing roughly spherical shaped in the size range between 15 nm – 20 nm. These results on size and distribution supplemented with the SEM results (figure 3). The smaller size of SPIONs were evenly reported where Justin *et al* (2018) stated SPIONs of size 15 nm and Samrot *et al* (2019c) detailed the SPIONs produced of 20 nm in size when NaOH was used as the reducing agent.

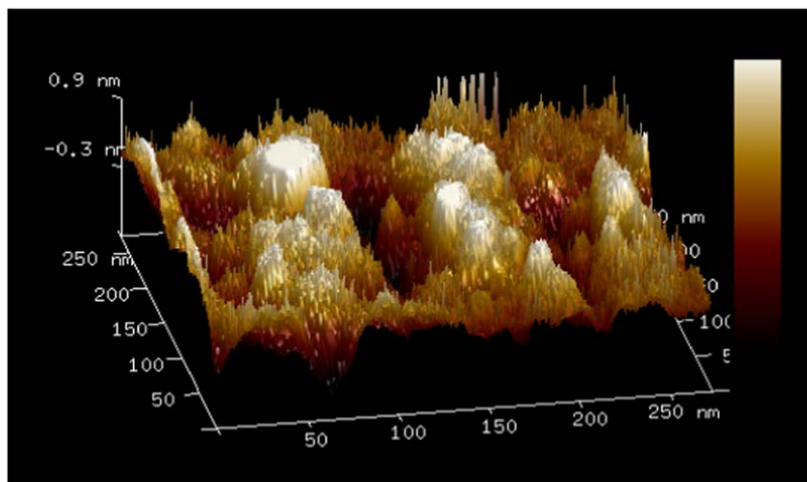
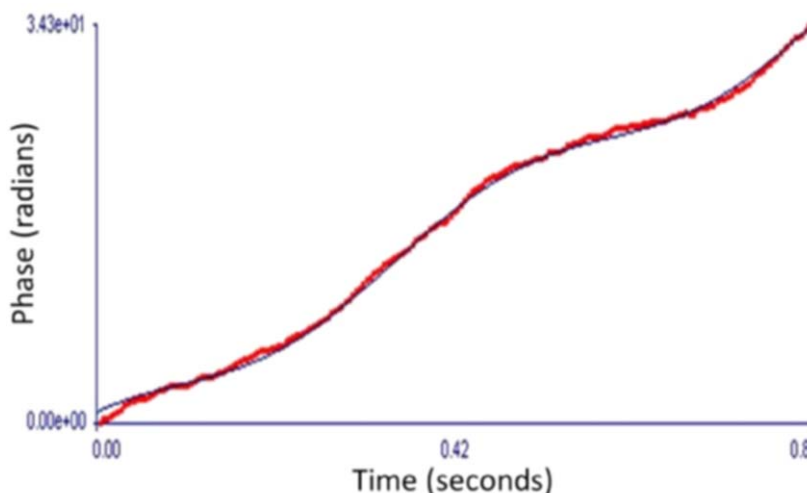


Figure 4. AFM analysis of SPIONs.



Run	Mobility	Zeta Potential (mV)	Rel. Residual
1	-1.13	-14.42	0.0233
2	-1.23	-15.70	0.0165
Mean	-1.18	-15.06	0.0199
Std. Error	0.05	0.84	0.0034
Combined	-1.18	-15.05	0.0165

Figure 5. Zeta potential analysis of SPIONs.

### 3.1.4. AFM

The 3D illustrative image of the synthesized SPIONs was seen with the help of AFM which recorded the size to be around 15 nm, which further supported the TEM and SEM results (figure 4).

### 3.1.5. Zeta potential analysis

The particle stability detected through the charge distribution on the surface of the synthesized SPIONs exhibited the zeta potentials as  $-15$  mV (figure 5). The values such as these indicate that the particles are stable with negative surface charge. Nanoparticles are said to be stable when their zeta potential values are greater than  $+25$  mV or less than  $-25$  mV(Justin et al 2018).

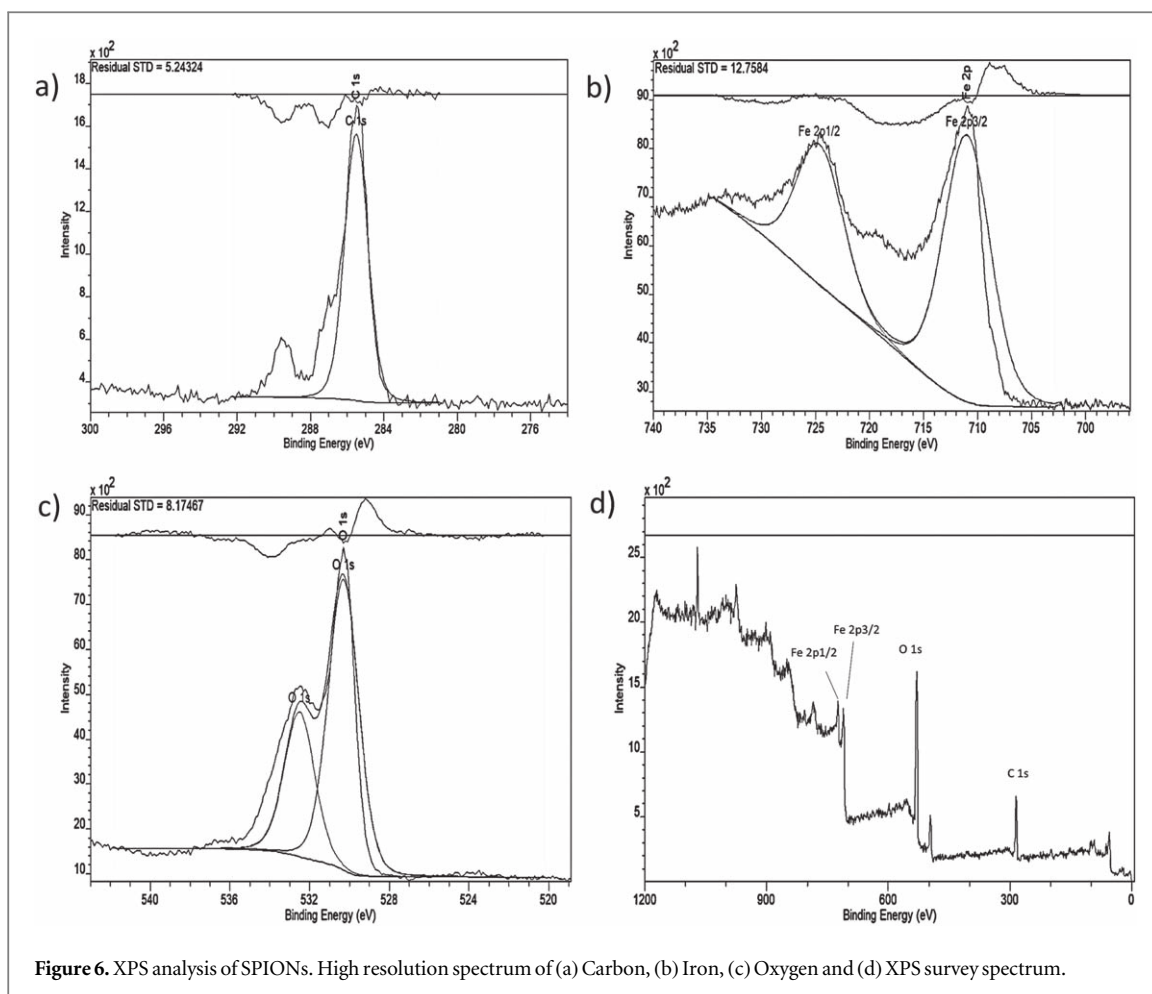


Figure 6. XPS analysis of SPIONs. High resolution spectrum of (a) Carbon, (b) Iron, (c) Oxygen and (d) XPS survey spectrum.

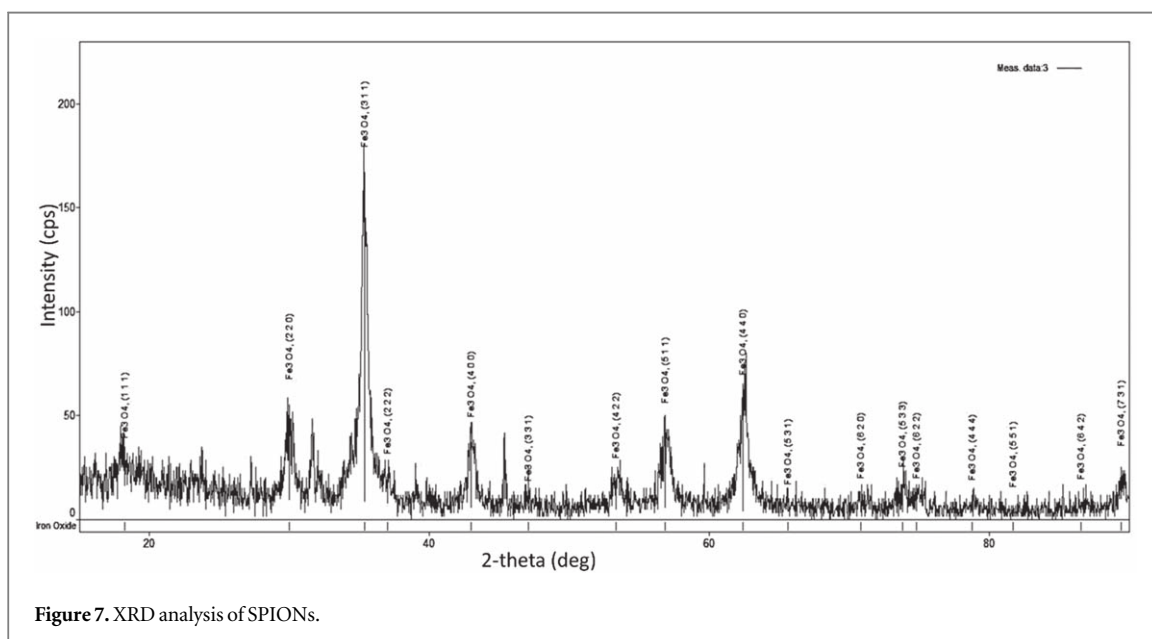
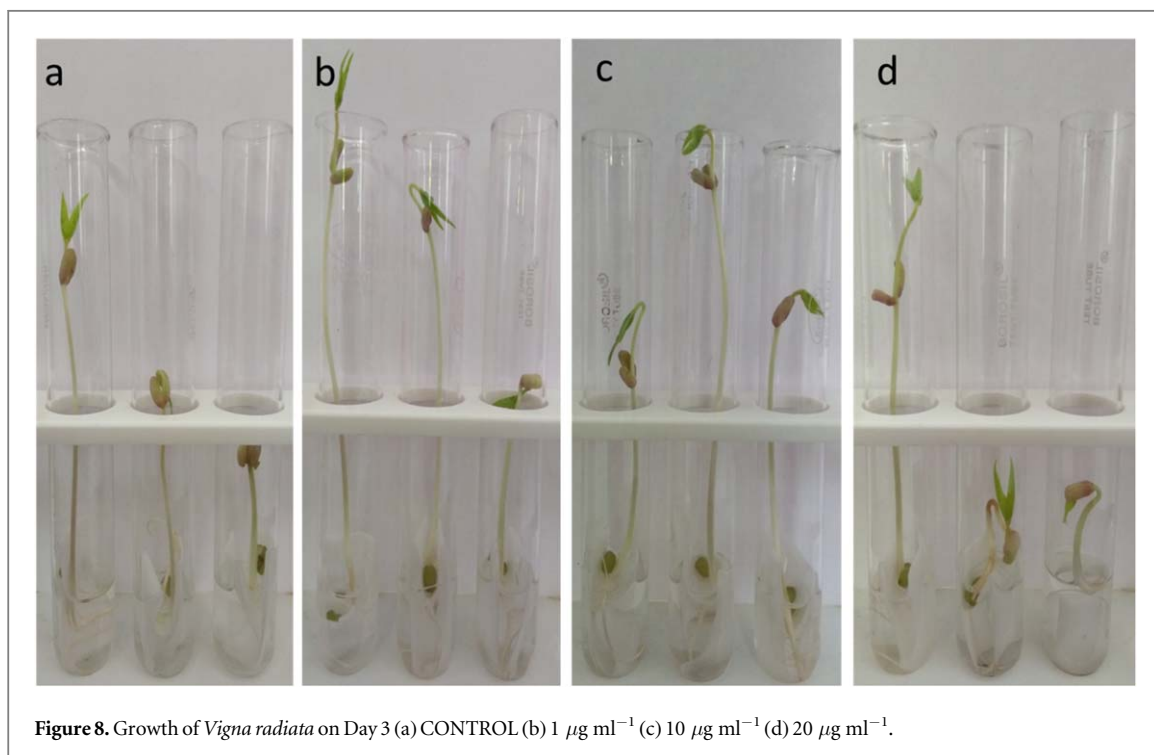


Figure 7. XRD analysis of SPIONs.

### 3.1.6. XPS

From the obtained records of XPS, the binding energy of Fe was recognized at 710 eV and the binding energy of CO and O was at 285.0 eV and 533.0 eV respectively (figure 6), which was showing it to be Fe<sub>3</sub>O<sub>4</sub>. Samrot *et al* (2018d) has also reported the characteristics of Fe<sub>3</sub>O<sub>4</sub> as the binding energy at 711.8 eV, FeO at 709.6 eV and Fe





**Figure 8.** Growth of *Vigna radiata* on Day 3 (a) CONTROL (b)  $1 \mu\text{g ml}^{-1}$  (c)  $10 \mu\text{g ml}^{-1}$  (d)  $20 \mu\text{g ml}^{-1}$ .

at 706.7 eV. By fitting the XPS data in Shirley background subtraction using the CASAPEAK software, the high-resolution spectrum of C 1s, O 1s, Fe 2p<sub>3/2</sub> and Fe 2p<sub>1/2</sub> were represented.

### 3.1.7. XRD

The XRD diffractogram with sharp peaks signify high crystalline nature of the synthesized particle. The diffraction peaks of  $2\theta$  with the planes at (220), (311), (400), (511), and (440) figure 7 corresponds to cubic spinel arrangement of  $\text{Fe}_3\text{O}_4$  (JCPDS 85-1436). This is more comparable with the XRD data of SPIONs in our earlier report (Samrot *et al* 2018d).

Using the below Debye–Scherrer equation, the crystallite size was calculated.

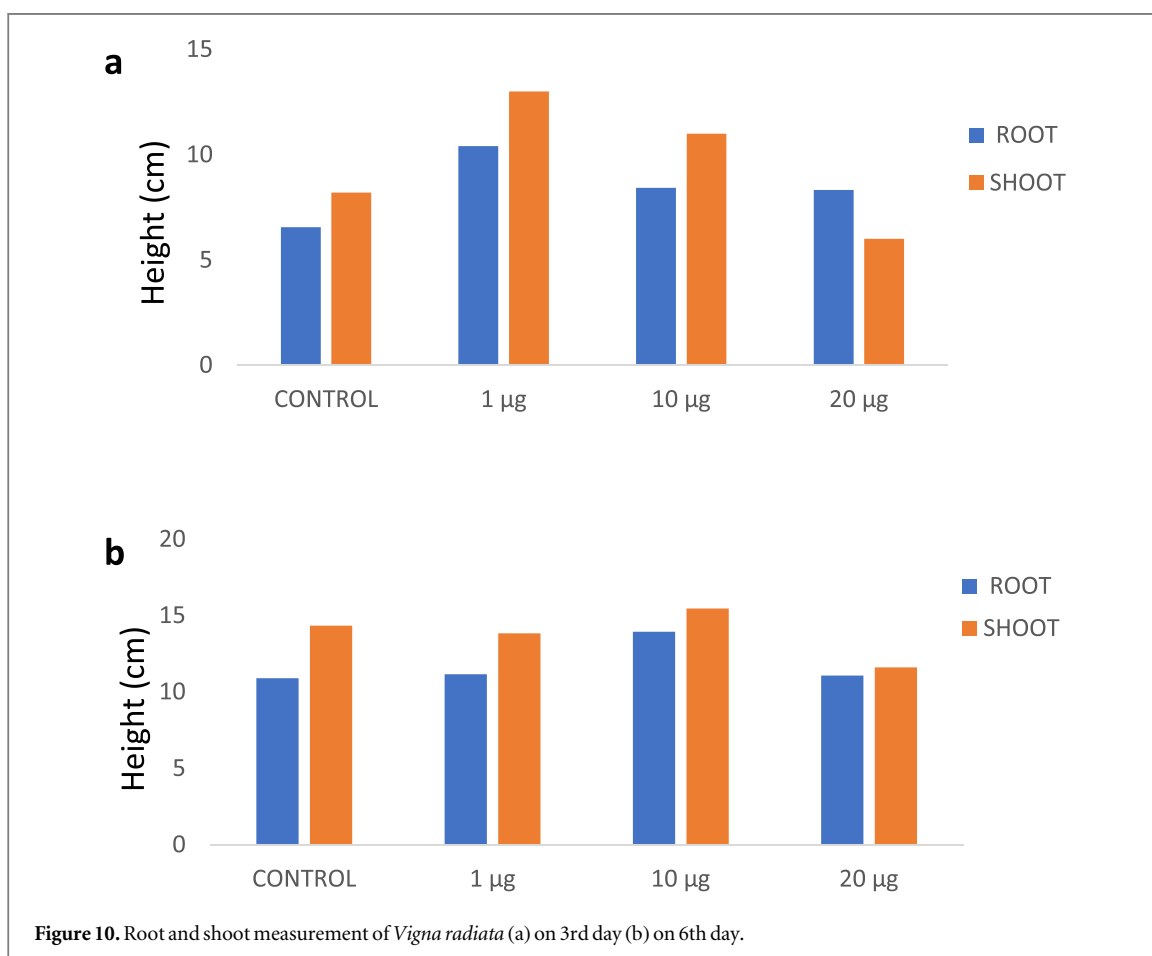
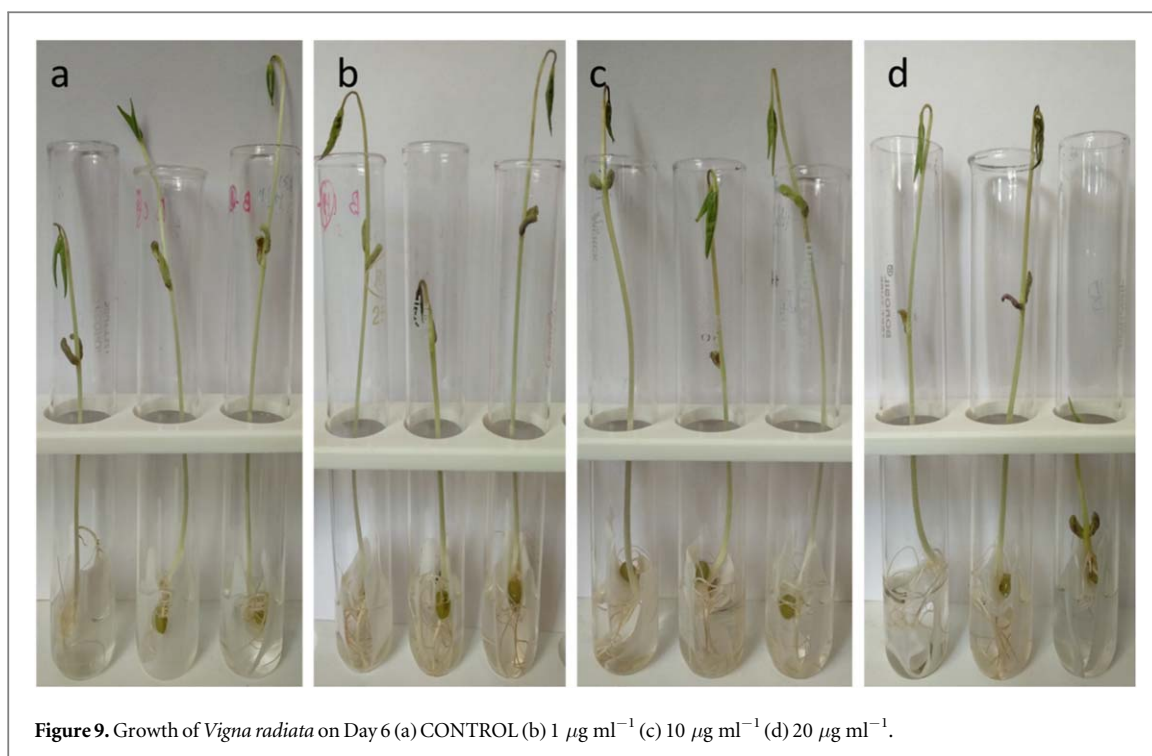
$$D = \frac{K\lambda}{\beta \cos \theta}$$

where K is known as constant which is equal to 0.90,  $\theta$  represents the Bragg angle,  $\lambda$  represents the wavelength of the incident x-ray used ( $\lambda = 0.1540 \text{ nm}$ ),  $\beta$  is Full Width at Half Maximum (FWHM) of the sharp peak recorded from the XRD analysis. The high intensity sharp peaks were considered in order to calculate the average crystallite size. It was found to be 11.97 nm. The maximum diffraction peak at plane (311) with FWHM of  $0.521^\circ$  corresponded to crystallite size of 15.98 nm. This further supports the results of AFM (15 nm) which is a 3D imaging. Thus the size of each crystal or grain of SPIONs was understood from XRD.

## 3.2. Impact of SPIONs on plant growth

### 3.2.1. Root and shoot measurement

The effect of SPIONs on root and shoot development was examined by measuring their growth in centimeter (cm). *Vigna radiata* plants were measured on 3rd and 6th day. The minimal concentration ( $1 \mu\text{g ml}^{-1}$  and  $10 \mu\text{g ml}^{-1}$ ) exposure has led to biostimulation in treated plants showing increased growth in root and shoot compared to control, expressing a maximum growth of 13:10.4 (shoot : root) by  $1 \mu\text{g ml}^{-1}$  treated plants (figures 8 and 10(a)). And also, optimistic impact as numerous rootlets development was evident with  $1 \mu\text{g ml}^{-1}$  and  $10 \mu\text{g ml}^{-1}$  treated *Vigna radiata* which is on par with the results of Shankramma *et al* (2016) who stated an enhanced growth in iron oxide treated *Solanum lycopersicum* owing to biomineralization and has also identified the deposition of iron oxides on the root hairs, root tips and nodal regions of treated plants. While the prolonged exposure (4–6 days) at the minimal concentration ( $1 \mu\text{g ml}^{-1}$  and  $10 \mu\text{g ml}^{-1}$ ) did not influence the growth of treated plants effectively as compared to the control which showed progressive growth (figures 9 and 10(b)). However, there was reduction in root development in  $20 \mu\text{g ml}^{-1}$  exposed groups. Similar report has been discussed by Bombin *et al* (2015), where they studied the iron oxide nanoparticles ( $\text{Fe}_2\text{O}_3$ ) with different charge coatings on *Arabidopsis thaliana* to hinder the root and shoot growth with reduced pollen viability, distressing its reproducing ability. Conversely, Iannone *et al* (2016) has exposed citric acid coated  $\text{Fe}_3\text{O}_4$  nanoparticles on



*Triticum aestivum* under hydroponic condition and reported null effect of  $\text{Fe}_3\text{O}_4$  on plant growth and germination but reported an increased activity of antioxidant enzymes. Lin and Xing (2007) experimented with zinc oxide nanoparticle in higher plants and concluded with termination of root elongation in radish, grape and ryegrass.

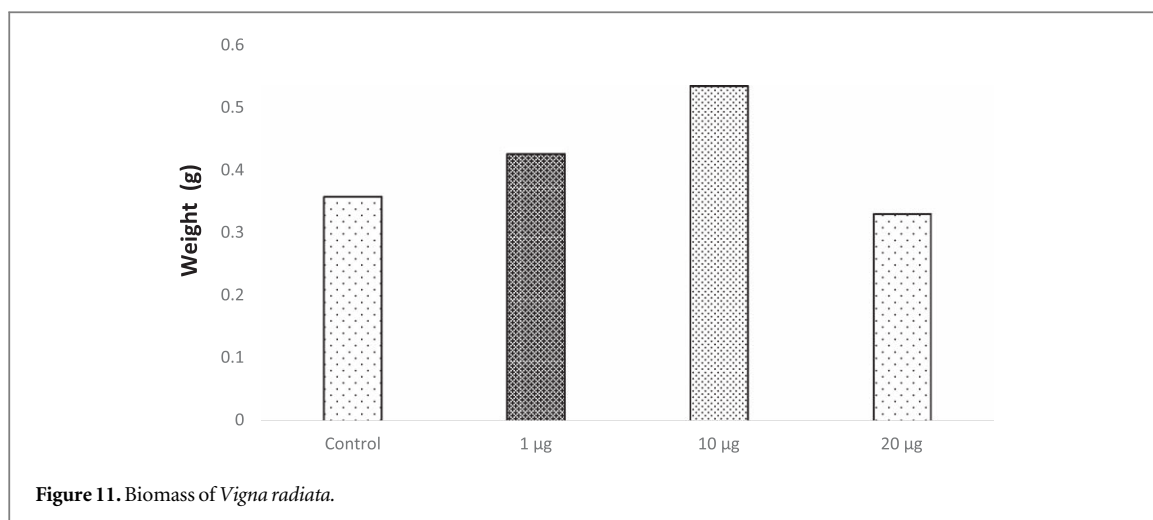


Figure 11. Biomass of *Vigna radiata*.

Table 1. Phytochemicals screening in *Vigna radiata*.

Phytochemicals	Control	1 µg ml <sup>-1</sup>	10 µg ml <sup>-1</sup>	20 µg ml <sup>-1</sup>
Carbohydrates	+	+	+	+
Protein	+	+	+	+
Lipids	+	+	+	+
Flavonoids	+	+	+	+
Tannins	-	-	-	-
Saponins	+	+	+	+
Glycosides	+	+	+	+
Phenols	-	-	-	-
Alkaloids	-	-	-	-

'+' indicates presence.

'-' indicates absence.

### 3.2.2. Biomass evaluation

The plantlets of *Vigna radiata* were checked for their biomass content soon after the treatment with SPIONs and it was found that the plants treated with 1 µg ml<sup>-1</sup> and 10 µg ml<sup>-1</sup> of SPIONs showed maximum biomass of 0.426 g/plant and 0.53 g/plant respectively when compared to the control (0.358 g ml<sup>-1</sup>) (figure 11). This could be due to the growth stimulation factor of SPIONs in treated *Vigna radiata*. Wang et al (2015) reported that nano-ferric oxides at 20 mg l<sup>-1</sup> on *Citrullus lanatus* showed increased soluble protein and chlorophyll contents. It could possibly infer that iron oxide nanoparticles at low concentrations are likely to promote the quality of the treated plants conversely the effect is stumpy at higher concentrations (20 µg ml<sup>-1</sup>) on treated *Vigna radiata* plantlets. From the observations and results, it can be deduced that the quality of the plants were affected by the presence of SPIONs. Ghodake et al (2011) also stated a comparable result where cobalt and zinc oxide nanoparticles have inhibited the root elongation in *Allium cepa* through bioaccumulation causing severe hazardous effect at cellular and chromosomal levels. Although Rui et al (2016) have supported that the use of iron oxide nanoparticles as iron fertilizers on *Arachis hypogaea*, a crop sensitive to iron deficiency had evidently showed increased root length, plant height, higher biomass, phytohormone contents and antioxidant enzyme activity, the prolonged exposure and long term usage may lead to risk associated with biomagnification, which are needed to be studied in field conditions.

### 3.2.3. Phytochemical screening

The phytochemical analysis of treated *Vigna radiata* indicated the presence of carbohydrates, protein, lipids, flavonoids, saponins, glycosides and the absence of phenols, tannins and alkaloids were observed (table 1).

### 3.2.4. Prussian blue staining of plant tissues

Accumulation of iron oxide particles was observed in all the test groups, where higher concentrations were found in the cortex of roots and stem (figures 12 and 13(b)–(d)), iron oxide particles were even found inside the

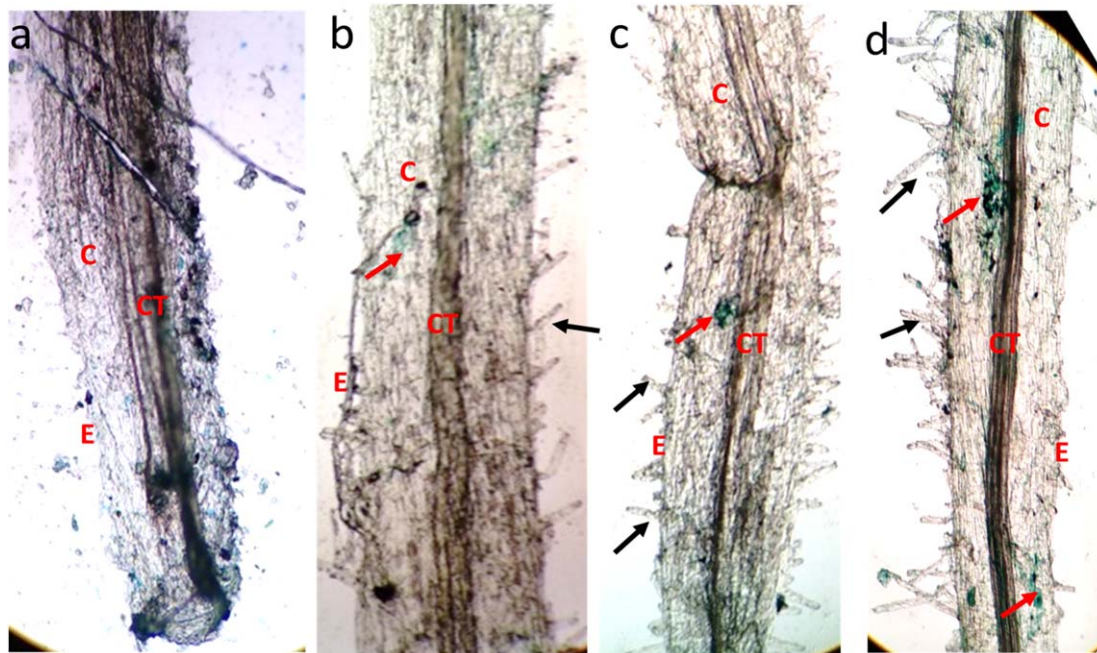


**Figure 12.** Microscopic imaging of Prussian blue stained root (a) Control (b)  $1 \mu\text{g ml}^{-1}$  (c)  $10 \mu\text{g ml}^{-1}$  (d)  $20 \mu\text{g ml}^{-1}$ . E—epidermis, CT—connective tissue, C—cortex, black arrow—root hair, red arrow—iron oxide presence.

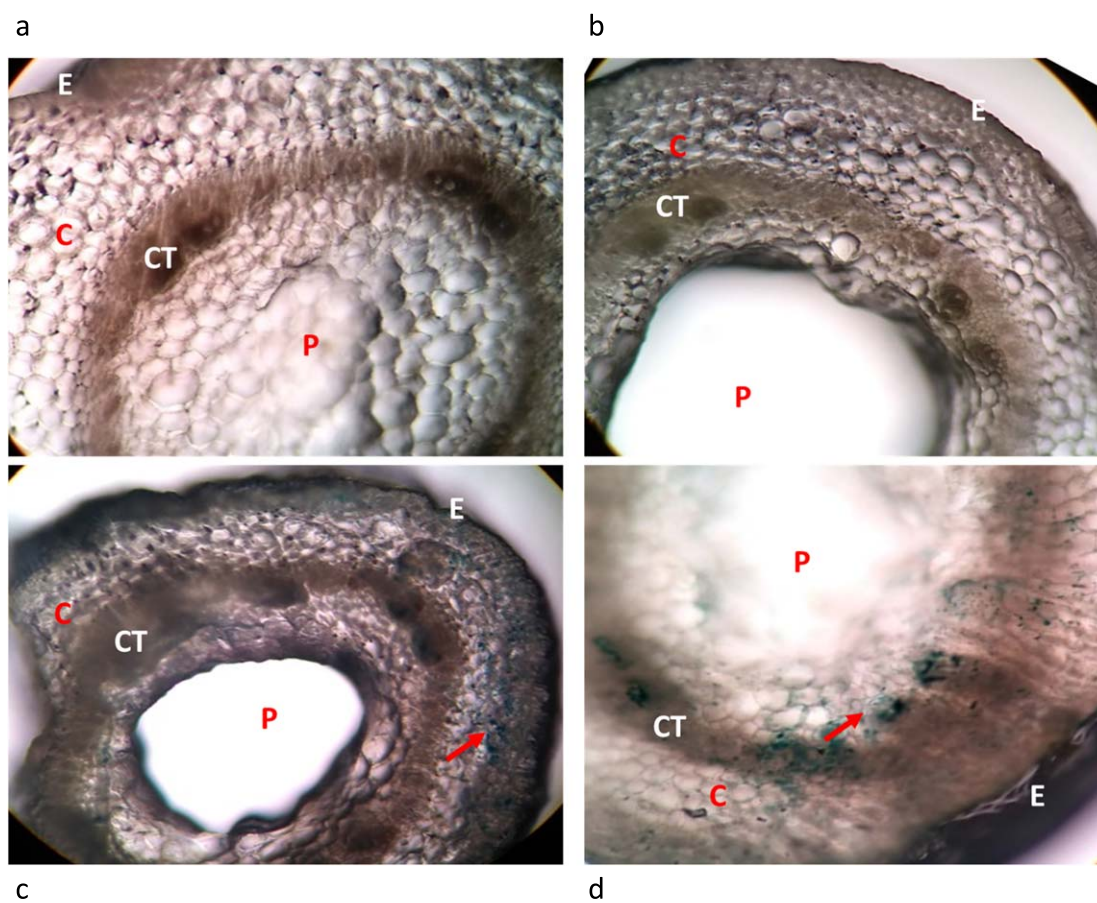


**Figure 13.** C.S of Prussian blue stained stem (a) Control (b)  $1 \mu\text{g ml}^{-1}$  (c)  $10 \mu\text{g ml}^{-1}$  (d)  $20 \mu\text{g ml}^{-1}$ . E—epidermis, C—Cortex, CT—connective tissue, P—pith black arrow—abnormality in pith, red arrow—iron oxide presence.

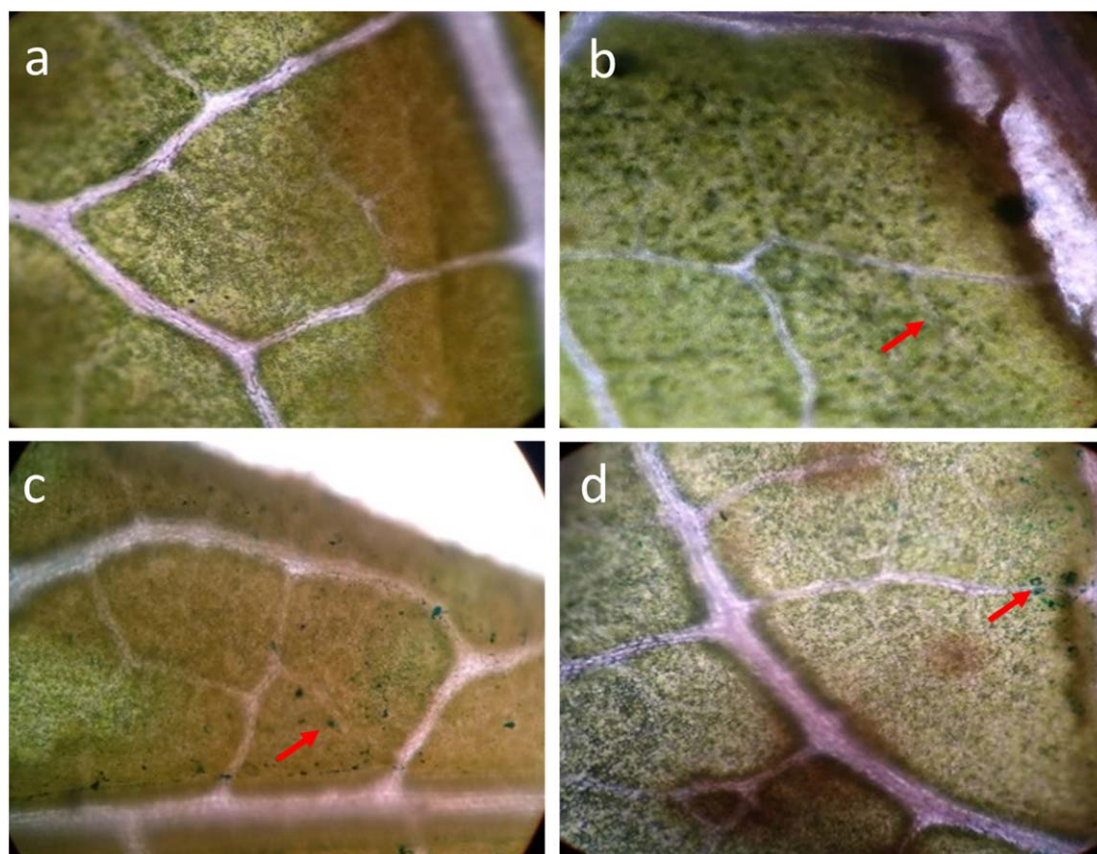


**Figure 14.** Microscopic image of Prussian blue stained leaves (a) Control (b)  $1 \mu\text{g ml}^{-1}$  (c)  $10 \mu\text{g ml}^{-1}$  (d)  $20 \mu\text{g ml}^{-1}$  red arrow—iron oxide presence.

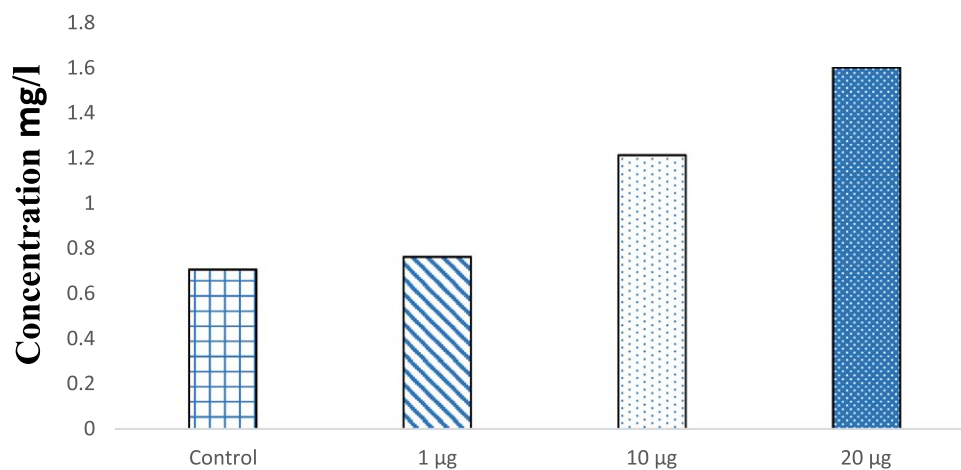


**Figure 15.** ICP-OES of SPIONs treated plant tissue.

leaves (figure 14). Prussian blue staining has been used to identify the uptake of iron by plants (Rios *et al* 2016). It is obvious from the SPIONs accumulated in tissues of plants might pave way for bioaccumulation.

### 3.2.5. ICP-OES of *Vigna radiata*

The incorporation of iron oxide into the plant tissues were further confirmed by ICP-OES. The study detected the highest iron content of  $1.59 \text{ mg l}^{-1}$  in  $20 \mu\text{g ml}^{-1}$  treated plants, followed by  $10 \mu\text{g ml}^{-1}$  having  $1.21 \text{ mg l}^{-1}$  and  $1 \mu\text{g ml}^{-1}$  with  $0.76 \text{ mg l}^{-1}$  while the control having  $0.705 \text{ mg l}^{-1}$  of Fe (figure 15). The presence of Fe in control must be the natural mineral composition in the seeds. Raju *et al* (2016) have also used *Vigna radiata* as

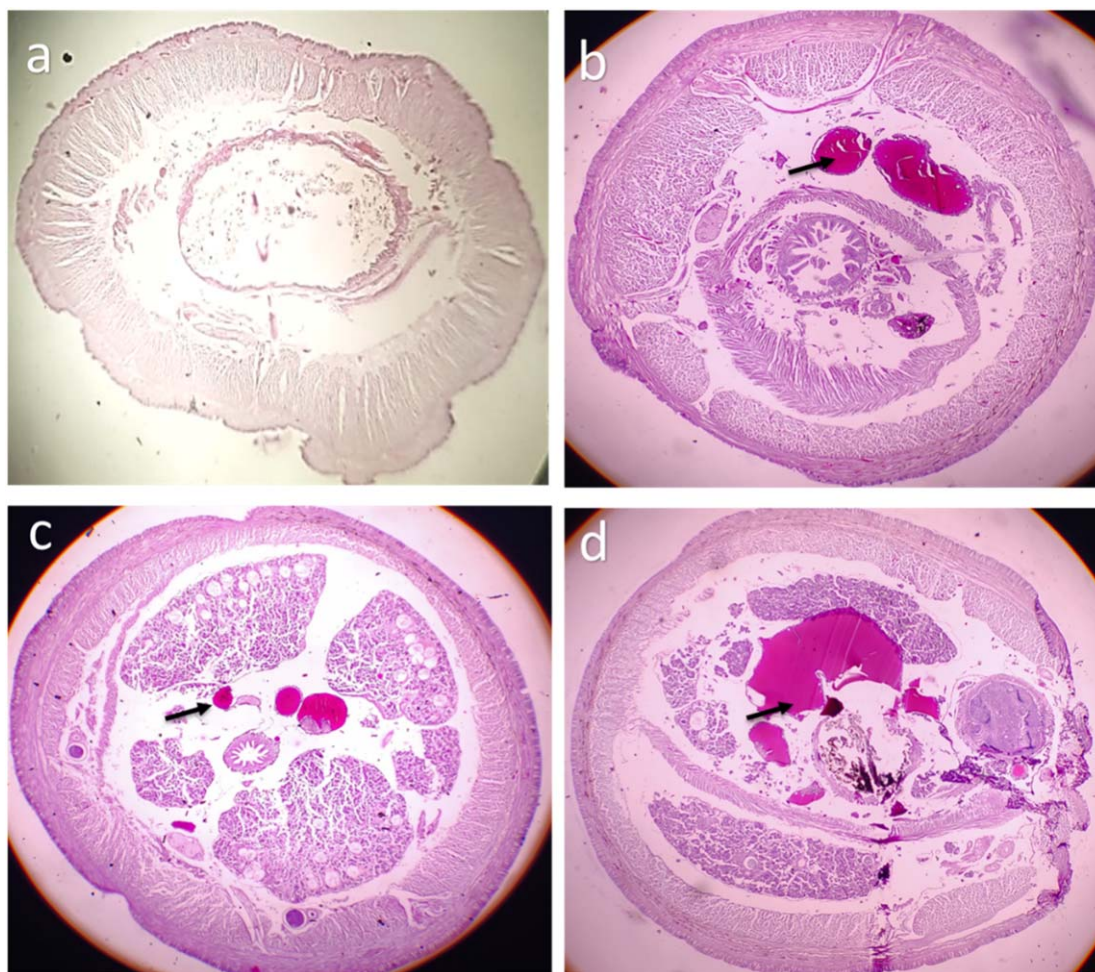


**Figure 16.** Histology image of earthworm foregut-SPIONs (a) control (b) exposed to 10  $\mu\text{g}$  SPIONs (c) exposed to 20  $\mu\text{g}$  SPIONs (d) exposed to 30  $\mu\text{g}$  SPIONs. black arrows denote lipofuscin deposits.

**Table 2.** Population study of earthworms before and after the SPIONs exposure.

Concentration No. of earthworms	Control		10 mg		20 mg		30 mg	
	Before	After	Before	After	Before	After	Before	After
	20	53	20	46	20	45	20	40

the plant model to study the effect of iron oxide nanoparticles and detected the uptake of iron oxide nanoparticles by the plant tissue through ICP-MS analysis.

### 3.3. Impact of SPIONs on *Eudrilus eugeniae*

#### 3.3.1. Effect on phenotypic character and reproduction

Due to the accumulation of SPIONs in the epithelium of earthworms, the color of the Earthworm was found to get darker with increasing concentrations but no mortality was observed in the Earthworms, Samrot *et al* (2017, 2018b) also reported similar observations when earthworms were exposed to magnetite and gold nanoparticles. The accumulation of nanoparticles has also affected the reproduction rate of earthworms. The reproduction rate was highly affected as the concentration increased table 2. Gold nanoparticles and silver nanoparticles were also found to reduce the number of earthworms after exposure. (Samrot *et al* 2018c, 2018e).

#### 3.3.2. Histology studies

The histology images have revealed adverse effects of SPIONs caused on the tissues of earthworms. Impact of SPIONs in the gut region was evidenced by disintegration of the gut and lipofuscin deposits (figure 16). The

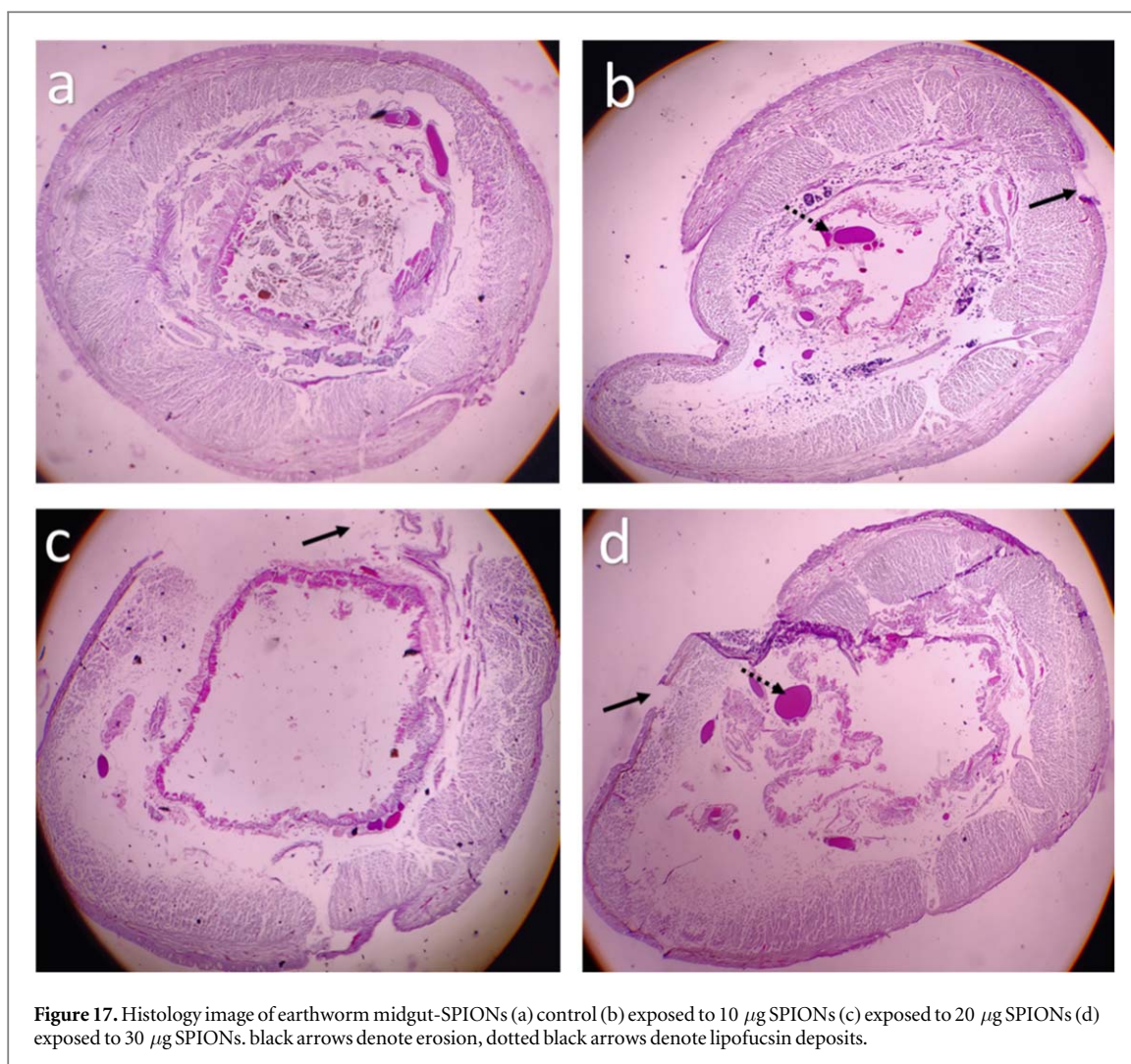


**Figure 17.** Histology image of earthworm midgut-SPIONs (a) control (b) exposed to 10  $\mu\text{g}$  SPIONs (c) exposed to 20  $\mu\text{g}$  SPIONs (d) exposed to 30  $\mu\text{g}$  SPIONs. black arrows denote erosion, dotted black arrows denote lipofuscin deposits.

outer structure of earthworm revealed drastic changes (figure 17). As the concentration of the Earthworms increased, erosion in circular and longitudinal muscle was observed (figures 16–18). And a complete destruction of gizzard area was also seen (figure 18(d)). Similar effects were observed in earthworms exposed to iron oxide, silver and gold nanoparticles causing disintegration of gut and other adverse effects in the Earthworms (Schlich *et al* 2013, Samrot *et al* 2018c, Samrot *et al* 2018e, ). The effect of carbon nanotubes along with sodium pentachlorophenol caused DNA and membrane damage on earthworms (Yang *et al* 2017).

### 3.3.3. ICP-OES of *Eudrilus eugeniae*

Accumulation of SPIONs into the treated earthworms can be witnessed with increase in concentration of nanoparticle. Accumulation of SPIONs in the control earthworms may be due to the nanoparticles present in the soil naturally (Samrot *et al* 2017). But the increased accumulation with increase in concentration (figure 19) explains that the effects noted are due to the nanoparticle ingestion.

## 4. Conclusion

In this study, SPIONs were produced by coprecipitation method in the presence of cobalt chloride. The nanoparticle size was found to be between 15 nm and 20 nm with crystalline nature and negative surface charge. On assessing the impact of synthesized SPIONs on *Vigna radiata*, it was found to increase the growth in treated plants at 1  $\mu\text{g ml}^{-1}$  and 10  $\mu\text{g ml}^{-1}$  concentration. High biomass and enormous rootlets formation were evident with 1  $\mu\text{g ml}^{-1}$  and 10  $\mu\text{g ml}^{-1}$  treated plants than control. The subcellular accumulation of SPIONs was visualized by Prussian blue staining. The successful uptake of SPIONs into the treated plant tissues have also been witnessed through ICP-OES analysis. Though there was growth stimulating effect initially, the prolonged exposure has rendered undesirable influence on the treated plants. In *Eudrilus eugeniae*, SPIONs exposure affected the appearance and the reproduction rate of treated earthworm with the increase in concentration. The

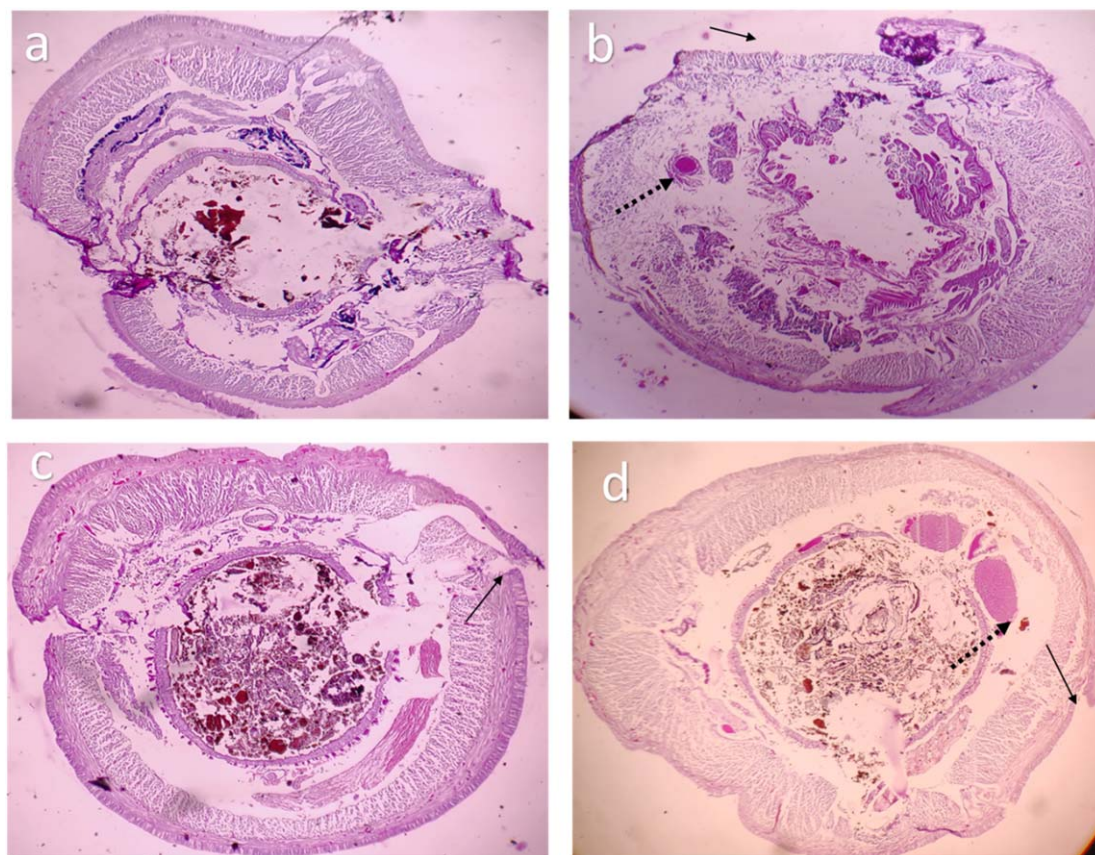


**Figure 18.** Histology image of earthworm hindgut-SPIONs (a) control (b) exposed to 10  $\mu\text{g}$  SPIONs (c) exposed to 20  $\mu\text{g}$  SPIONs (d) exposed to 30  $\mu\text{g}$  SPIONs. black arrows denote erosion, dotted black arrows denote lipofuscin deposits.

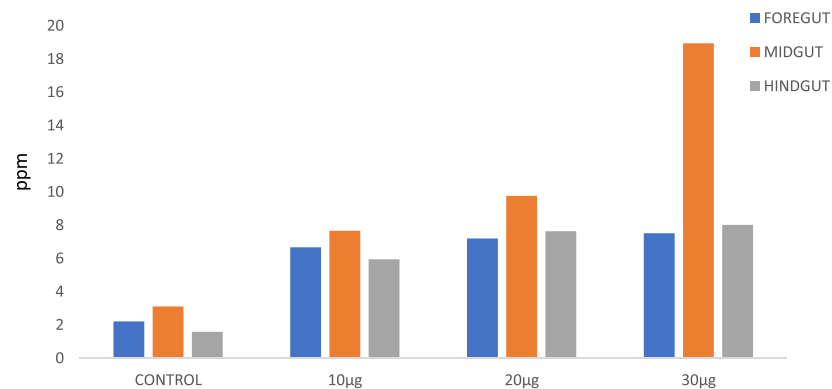


**Figure 19.** ICP-OES analysis of earthworms.

disintegration of gut and lipofuscin deposits were noticed through histological studies and the accumulation of SPIONs into the Earthworms were detected through ICP-OES. Thus, nanoparticles are said to cause toxic effects to the environment and hence proper disposal methods are required. Mostly the iron oxides are not stable at higher temperatures and so they can be disposed by incineration.

### Conflict of interest

The authors declare that they have no conflict of interest.



## Funding

This research did not receive any specific grant from funding agencies in the public, commercial, or not-for-profit sectors.

## ORCID iDs

Antony V Samrot  <https://orcid.org/0000-0001-9536-0567>

## References

- Ahamed M, Alsalmi M S and Siddiqui M K J 2010 Silver nanoparticle applications and human health *Clin. Chim. Acta* **411** 1841–8
- Auwal M S, Saka S, Mairiga I A, Sanda K A, Shuaibu A and Ibrahim A 2014 Preliminary phytochemical and elemental analysis of aqueous and fractionated pod extracts of *Acacia nilotica* (Thorn mimosa) *Vet Res Forum*. **5** 95–100
- Bombin S, Lefebvre M, Sherwood J, Xu Y, Bao Y and Ramonell K M 2015 Developmental and reproductive effects of iron oxide nanoparticles in *Arabidopsis thaliana* *Int. J. Mol. Sci.* **16** 24174–93
- Bulte J W M and Kraitchman D L 2004 Iron oxide MR contrast agents for molecular and cellular imaging *NMR Biomed.* **17** 484–99
- Butt K R and Lowe C N 2010 Controlled cultivation of endogeic and anecic earthworms *Biology of Earthworms* ed A Karaca 24 (Berlin, Heidelberg: Springer-Verlag Berlin Heidelberg) pp 107–12 ([https://link.springer.com/chapter/10.1007/978-3-642-14636-7\\_7](https://link.springer.com/chapter/10.1007/978-3-642-14636-7_7))
- Edeoga H O, Okwu D E and Mbaebie B O 2005 Phytochemical constituents of some Nigerian medicinal plants *Afr. J. Biotechnol.* **4** 685–8
- Ezeonu C S and Ejikeme C M 2016 Qualitative and quantitative determination of phytochemical contents of indigenous nigerian softwoods *New Journal of Science* **56013279**
- Geisler-Lee J, Wang Q, Yao Y, Zhang W, Geisler M, Li K, Huang Y, Chen Y, Kolmakov A and Ma X 2012 Phytotoxicity, accumulation and transport of silver nanoparticles by *Arabidopsis thaliana* *Nanotoxicology*. **7** 323–37
- Ghodake G, Seo Y D and Lee D S 2011 Hazardous phytotoxic nature of cobalt and zinc oxide nanoparticles assessed using *Allium cepa* *J. Hazard. Mater.* **186** 952–5
- Iannone M F, Groppa M D, De-Sousa M E, Raap M B F V and Benavides M P 2016 Impact of magnetite iron oxide nanoparticles on wheat (*Triticum aestivum* L.) development: evaluation of oxidative damage *Environ. Exp. Bot.* **133** 77–88
- Justin C, Philip S A and Samrot A V 2017 Synthesis and characterization of superparamagnetic iron-oxide nanoparticles (SPIONs) and utilization of SPIONs in x-ray imaging *Appl Nanosci* **7** 463–75
- Justin C, Samrot A V, Sruthi P D, Sahithya C S, Bhavya K S and Saipriya C 2018 Preparation, characterization and utilization of coreshell superparamagnetic iron oxide nanoparticles for curcumin delivery *PLoS One* **13** e0200440
- Kreuter J, Rameg P, Petrov V, Hamm S, Gelperina S E, Engelhardt B, Alyautdin R, Von-Briesen H and Begley D J 2003 Direct evidence that polysorbate-80-coated poly (butylcyanoacrylate) nanoparticles deliver drugs to the CNS via specific mechanisms requiring prior binding of drug to the nanoparticles *Pharm. Res.* **20** 409–16
- Kumar A, Sharma G, Naushad M and Thakur S 2015 Spion/ $\beta$ -cyclodextrin core-shell nanostructures for oil spill remediation and organic pollutant removal from waste water *Chem. Eng. J.* **280** 175–87
- Kumari R, Singh J S and Singh D P 2016 Biogenic synthesis and spatial distribution of silver nanoparticles in the legume mung bean plant (*Vigna radiata* L.) *Plant PhysiolBiochem.* **110** 158–66
- Lin D and Xing B 2007 Phytotoxicity of nanoparticles: inhibition of seed germination and root growth *Environ. Pollut.* **150** 243–50
- Osaka T, Nakanishi T, Shanmugam S, Takahama S and Zhang H 2009 Effect of surface charge of magnetite nanoparticles on their internalization into breast cancer and umbilical vein endothelial cells *Colloids Surf. B* **71** 325–30
- Praven R P and Nair A S 2014 Preliminary phytochemical screening of root extracts of *Myxopyrum milacifolium* blume *Asian Journal of Biomedical and Pharmaceutical Sciences* **4** 41–5
- Raju D, Mehta U J and Beedu S R 2016 Biogenic green synthesis of monodispersed gum kondagogu (*Cochlospermum gossypium*) iron nanocomposite material and its application in germination and growth of mung bean (*Vigna radiata*) as a plant model *IET Nanobiotechnol.* **10** 141–6
- Rios J J, Carrasco-Gil S, Abadia A and Abadia J 2016 Using perls staining to trace the iron uptake pathway in leaves of a prunus rootstock treated with iron foliar fertilizers *Front Plant Sci.* **7** 893
- Rui M et al 2016 Iron oxide nanoparticles as a potential iron fertilizer for peanut (*Arachis hypogaea*) *Front Plant Sci.* **7** 815
- Samrot A V, Akanksha, Tatipamula J, Padmanaban S, Sheryl-Ann P, Ujjala B and Rabel A M 2016 Chelators influenced synthesis of chitosan-carboxymethyl cellulose microparticles for controlled drug delivery *Appl. Nanosci.* **6** 1219–31
- Samrot A V, Angalene J L A, Roshini S M, Stefi S M, Preethi R, Raji P, Madankumar A, Paulraj P and Kumar S S 2019a Purification, characterization and utilization of polysaccharide of *Araucaria heterophylla* gum for the synthesis of curcumin loaded nanocarrier *Int. J. Biol. Macromol.* **140** 393–400
- Samrot A V, Bhavya K S, Sahithya C S and Sowmya N 2018c Evaluation of toxicity of chemically synthesised gold nanoparticles against *Eudrilus eugeniae* *J. Cluster Sci.* **29** 1217–25
- Samrot A V, Bhavya S K, Agnes J L A, Roshini S M, Preethi R, Stefi S M, Raji P and Kumar S S 2019b Utilization of gum polysaccharide of *Araucaria heterophylla* and *Azadirachta indica* for encapsulation of cyfluthrin loaded super paramagnetic iron oxide nanoparticles for mosquito larvicidal activity. *Int. J. Biol. Macromol.* accepted (<https://doi.org/10.1016/j.ijbiomac.2019.10.232>)
- Samrot A V, Justin C, Padmanaban S and Burman U 2017 A study on the effect of chemically synthesized magnetite nanoparticles on earthworm: *Eudrilus eugeniae* *Appl Nanosci.* **7** 17–23
- Samrot A V, Mathew A, Shylee L, Hemalatha N and Karunya A 2010 Evaluation of bioactivity of various Indian medicinal plants—an *in-vitro* study *The Internet Journal of Internal Medicine* **8** 1–9
- Samrot A V, Raji P, Selvarani A J, Sruthi P D, Angalene J L A, Ponnaiah P and Iyappan P 2019 *A Handbook on Phytochemical Extraction, Screening and its in-vitro Bioactivity Assays* (India: SARAS Publisher)
- Samrot A V, Sahithya C S, Selvarani A J, Pachiyappan S and Kumar S S 2019c Surface-engineered super-paramagnetic iron oxide nanoparticles for chromium removal *International Journal of Nano Medicine* **2019** 8105–19
- Samrot A V, Saipriya C, Agnes L A, Roshini S M, Cypriyana P J, Saigeetha S, Raji P and Kumar S 2019d Evaluation of nanotoxicity of *Araucaria heterophylla* gum derived green synthesized silver nanoparticles on *Eudrilus eugeniae* and *Danio rerio* *J Clust Sci.* **30** 1017–24

- Samrot A V, Senthilkumar P, Rashmitha S, Veera P and Sahithya C S 2018a *Azadirachtaindica* influenced biosynthesis of superparamagnetic ironoxide nanoparticles and their applications in tannery water treatment and x-ray imaging *J Nanostructure Chem.* **8** 343–51
- Samrot A V, Shobana N and Jenna R 2018b Antibacterial and antioxidant activity of different staged ripened fruit of *Capsicumannuum* and its green synthesized silver nanoparticles *Bionanoscience.* **8** 632–46
- Samrot A V, Shobana N, Sruthi P D and Sahithya C S 2018d Utilization of chitosan-coated superparamagnetic iron oxide nanoparticles for chromium removal *Appl Water Sci.* **8** 192
- Samrot A V, Ujjala B, Padmanaban S, Yamini P and Rabel A M 2018e A study on toxicity of chemically synthesised silver nanoparticle on *Eudriluseugeniae* *Toxicology and Environmental Health Sciences* **10** 162–7
- Schlich K, Klawonn T, Terytze K and Hund K R 2013 Hazard assessment of a silver nanoparticle in soil applied via sewage sludge *Environmental Sciences Europe* **25** 1
- Shankamma K, Yallappa S, Shivanna M B and Manjanna J 2016 Fe<sub>2</sub>O<sub>3</sub> magnetic nanoparticles to enhance *s. lycopersicum* (tomato) plant growth and their biomineralization *Appl Nanosci.* **6** 983–90
- Sharifi S, Behzadi S, Laurent S, Forrest M L, Stroeve P and Mahmoudi M 2012 Toxicity of nanomaterials *Chem. Soc. Rev.* **41** 2323–43
- Sruthi P D, Sahithya C S, Justin C, SaiPriya C, Bhavya K S, Senthilkumar P and Samrot A V 2019 Utilization of chemically synthesized super paramagnetic iron oxide nanoparticles in drug delivery, imaging and heavy metal removal *J. Cluster Sci.* **30** 11–24
- Taghavi S M, Momenpor M, Azarian M, Ahmadian M, Souri F, Taghavi S A, Sadeghain M and Karchani M 2013 Effects of nanoparticles on the environment and outdoor workplaces *Electron Physician.* **5** 706–12
- Wang M, Liu X, Hu J, Li J and Huang J 2015 Nano-ferric oxide promotes watermelon growth *J BiomaterNanobiotechnol.* **6** 160–7
- Wei H, Yang H B, Ciesielski P N, Donohoe B S, Mccann M C, Murphy A S, Peer W A, Ding S Y, Himmel M E and Tucker M P 2015 Transgenic ferritin overproduction enhances thermochemical pretreatments in *arabidopsis* *Biomass Bioenergy* **72** 55–64
- Xu H, Aguilar Z P, Yang L, Kuang M, Duan H, Xiong Y, Wei H and Wang A 2011 Antibody conjugated magnetic iron oxide nanoparticles for cancer cell separation in fresh whole blood *Biomaterials* **32** 9758–65
- Yang L et al 2008 Development of receptor targeted iron oxide nanoparticles for efficient drug delivery and tumor imaging *J Biomed Nanotech.* **4** 439–49
- Yang Y, Xiao Y, Li M, Ji F, Hu C and Cui Y 2017 Evaluation of complex toxicity of carbon nanotubes and sodium pentachlorophenol based on earthworm coelomocytes test *PLoS One* **12** 1